

# Implementation of Machine-Based Learning Solutions in Distance Education for Pathologists in Ophthalmic Oncology

Denis Garri  
A.I. Yevdokimov Moscow State  
University of Medicine and  
Dentistry  
Moscow, Russia  
Email: ldenisl@inbox.ru

Svetlana Saakyan, Inna  
Khoroshilova-Maslova,  
Alexander Tsygankov  
Helmholtz Moscow Research  
Institute of Eye Diseases  
Moscow, Russia  
Email: svsaakyan@yandex.ru  
horoshilova@yandex.ru  
alextsygankov1986@yandex.ru

Oleg Nikitin, Grigory Tarasov  
Limited Liability Company  
"Artificial Networks and  
Technologies"  
Moscow, Russia  
Email: olegnikitin@mail.ru  
grigoriy.tarasov.u@gmail.com

**Abstract** – Uveal melanoma is a malignant tumor originating from melanocytes of an eye vascular tract. Depending on the cellular composition, the tumor is classified as a spindle cell (A or B), epithelioid cell or mixed cell. The presence of epithelioid cells reflects an unfavorable vital prognosis. The study of the cellular composition of the tumor is subjective and results in disagreements about the type of individual cells in 13% of cases among qualified pathologists. The discrepancies in diagnoses are due to the use of different classifications, which can lead to an incorrect assessment of the vital prognosis and incorrect tactics of patient treatment. Machine learning can be used to objectify the criteria of pathomorphological study of uveal melanoma, but currently there are no published works on machine analysis of pathomorphological images of this type of tumors. Our solution is based on the use of conventional neural network for the classification of images of uveal melanoma cells. We obtained an average F-score value of 0.75 to differentiate spindle cells nuclei from epithelioid cells nuclei and developed a visualization interface to explain differences between various types of cells with color mark-up of cell nuclei, probability of belonging to a certain class and deconvolution maps.

**Keywords**-E-learning; artificial neural networks; pathology; uveal melanoma.

## I. INTRODUCTION

Uveal melanoma is the most common primary intraocular malignant tumor in the adult population [1]. Tumor cell dissemination is a frequent occurrence with uveal melanomas. Even with complete removal of the primary tumor, metastatic foci are detected in 50% of patients. In case of tumor metastasis, the vital prognosis is substantially worse, with the average survival rate during the first year falling to 20% [2].

The tumor cell type is an important prognostic factor. The McLean classification is used currently, including spindle-A, spindle-B, epithelioid and mixed tumors [3]. Studies have shown that spindle cell tumors offer the best vital prognoses, while for mixed cell tumors the outlook is

intermediate, and epithelioid cell tumors present the most unfavorable prospects. A greater number of epithelioid cells in the field of view is associated with a worse vital prognosis [4]. The morphological characteristic of the tumor composition is subjective, and the quantity of epithelioid cells required to identify tumors as epithelioid or mixed type has not yet been universally defined. Disagreements among qualified pathologists regarding belonging of individual melanoma cells to a certain type are on average 13%, which is due to the lack of objectively measurable signs and the presence of intermediate-type cells that have signs of several cell types. McLean and co-authors found that differences in the classifications used led to differences in diagnosis in 32% of cases [3]. Machine learning can be used to objectify the criteria of pathomorphological study of uveal melanoma.

The article is organized as follows. In Section II, we present the state of art concerning machine learning use in digital pathology. Section III discusses our training set, method specification and performance metrics. In Section IV, the use of the trained network is discussed. Finally, the paper is concluded in Section V.

## II. STATE OF ART

### A. Machine Learning

Machine learning is applied in every field of human activity where digital data is used. Various articles have been published recently concerning the use of artificial intelligence for the purposes of classification, regression and segmentation in medicine and particularly in pathology.

Machine learning and deep learning are self-learning methods used to analyze complex data and find patterns and interdependencies without explicit programming. Due to this, they are sometimes called "artificial intelligence".

Machine learning includes models and algorithms that mimic the architecture of biological neural networks. Artificial neural networks are of great interest in the field of

machine learning, particularly networks based on deep learning. This is due to their capacity for working effectively with complex and multidimensional databases, along with the increasing availability of databases and the performance of graphics processors.

### B. Digital Pathology

Recent developments in the field of digital pathology, related to the access of medical institutions to digital microscopes and slide scanners, allow us to carry out scientific work with digital data, including gigapixel images of pathological specimens. The availability of such data allows the use of a range of machine learning methods to process it and to obtain new unified diagnostic criteria and prognoses for the passage of malignant diseases that are unavailable in a classical pathology study [5]. Recent studies have shown that convolutional neural networks reveal a high accuracy in the identification of pathological images of certain types of cancer, including the pathology of the prostate gland, lung, mammary gland, large intestine, and ovaries [6]-[10]. The unit of learning is usually a small image of about 100x100 microns or larger. This approach is convenient to identify tissue patterns in the images under study and can be used to determine the predominant cell population in the image, but to characterize individual cells, the size of one image should be comparable to the size of one cell – 10-20 microns.

No published articles devoted to the machine analysis of pathomorphological images of uveal melanoma are available at the moment. The articles that are the closest to our work in terms of purpose and methodology are devoted to the study of images of melanoma of the skin, which, despite the similarity of origin, has a different metastatic potential, responds differently to treatment and has different immunological and genetic characteristics. The primary tumor focus of melanoma of the skin lies in the depth of the tissues of epidermal origin, and uveal melanoma – in the tissues of mesodermal origin, which results in their different histological characteristics [11].

Effland et al. provided variational networks to differentiate tumor nuclei from the nuclei of immune cells. Tissue samples were tinted with immunofluorescent dyes, giving a different color signal while interacting with CD45 antigen of immune cells, gp100 protein antigen of tumor cells and adenine–thymine rich regions in nuclei, which allowed to form a training sample without using a manual marking process [12]. In [13], Rexhepaj et al. used Melan-A dye for immune staining of melanoma cells; they created training samples of tumor and non-tumor cells and analysed them using support vector machine. This experiment can not be used to differentiate different types of uveal melanoma cells due to the fact that there are no dyes specifically staining epithelioid or spindle cells.

Liu et al. used SetSVM – support vector machine modification – to solve a number of diagnostic problems, in particular, the differentiation of dysplastic nevus from

malignant melanoma of the skin. The approach provided the use of cell nuclei features to categorize each case [14]. The method showed high accuracy in the classification of groups of homogeneous cells (up to 82.01%), but can not be used for mixed cell cases as well as to characterize individual cell elements.

Our contribution is to create and train an artificial convolutional neural network that would allow the less malignant cellular elements (spindle-shaped cells) to be distinguished from the most malignant (epithelioid cells). Determination of the cellular composition of a tumor is a routine event, but it is difficult to characterize individual cells, especially in mixed tumors. Our solution should help to improve the diagnostic skills of students and pathology specialists.

### III. ARTIFICIAL NEURAL NETWORK LEARNING PROCESS

The first stage of neural network training is the preparing of the training set. For this purpose, 52 patients who underwent enucleation from 2005–2006 were selected and their pathology reports and clinical records were studied. Being faced with the task of classification between two groups of cells, we selected for the training sample only those tumors that, according to the reports, were spindle or epithelioid. Inclusion in the training sample of mixed tumors would require labor-intensive process for marking various cells in the tumor site. The use of tumors with a homogeneous cell composition would allow the markup to be applied to the tumor site as a whole. According to current classifications, spindle cell tumors can contain up to 10% of epithelioid cells and vice versa, so we decided to evaluate the possibility of marking mainly homogeneous tumors after digitizing their histological slides.

By excluding mixed cell tumors from the training set, we had 23 patients and 37 histological slides for them. All samples were digitized using a Leica ScanScope CS2 slide scanner, producing 37 gigapixel images in .svs format. After reviewing the digitized images, we decided to use the following for further training set: 24 gigapixel images from 12 patients – spindle cell tumors; 4 gigapixel images from 3 patients – epithelioid cell tumors. In total, 28 images were used. Nine images from 8 patients could not be used in the training set since it proved impossible to isolate nodes of homogeneous cell composition. We plan to use the images not included in the training set for further control of the classifier.

Each gigapixel image was marked using Aperio ImageScope by a qualified pathologist. The marking was performed by complete encirclement of the tumor node with further exclusion from the marking area of non-tumor tissues and empty spaces. Convolutional neural networks require a large number of images in the training sample, so the problem of the small number of cases was solved by dividing the gigapixel images into smaller images of 240 x 240 pixels. The common term for such smaller images is a patch. One .svs image gave the output of a number of

patches from 2,573 to 57,554; the total number of patches was 605,375, with the average number of patches per image of 21,620.

The original files in .svs or .scn format are a set of pyramidal images. The base layer is 240x240 pixel images compressed using the libjpeg application library. The top layers comprise 4–16 images combined of lower layers with lost pixel density, up to the topmost image of approximately 2000x2000 pixels. Such a composition allows prompt navigation due to simultaneous displaying of approximately 10 small images instead of a number of images from the lower layer. Individual patches are extracted from a pyramidal image file using the same library.

For further processing, we scanned individual 240x240 patches with a 48x48 pixel scanning window, in increments of 8 pixels, and with an overlay round mask. Neural network ResNet-101 was used for image cell identification. The weight for the neural network was taken from weights which produced the best results on 2018 Data Science Bowl for cell nucleus localization [15]. During training, 48x48 pixel images with a round mask containing one cell were fed to another neural network input. The second neural network had 18,490 parameters and used the Adam(lr=0.01) optimizer and categorical\_crossentropy loss, as well as three Conv2D blocks:

- The first Conv2D block was composed of two foldings with 3x3 kernels, relu activation, BatchNormalization and dropout functions. The first Conv2D block had the convolution kernel size of 8, the first convolution stride of 2, and dropout rate of 0.2.
- The second Conv2D block had the convolution kernel size of 16, the first convolution stride of 2, and dropout rate of 0.4.
- The third Conv2D block had the convolution kernel size of 16, the first convolution stride of 2, and dropout rate of 0.4.

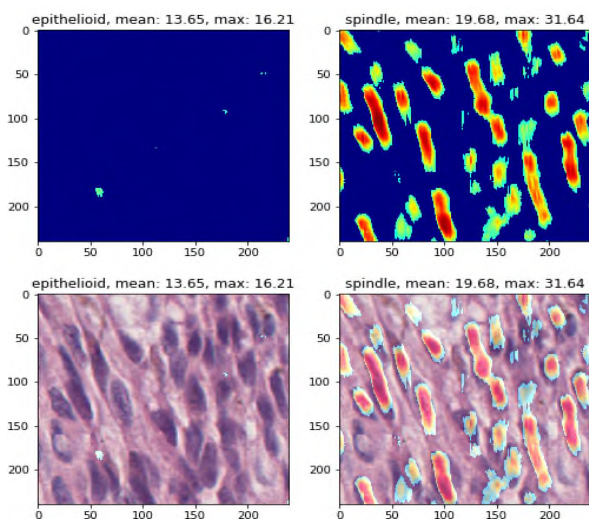


Figure 1. Mark-up of most and least probable nuclei location

Also, there are two fully connected layers with 32 parameters, relu activation, BatchNormalization and dropout functions. The last layer has two neurons and softmax activation.

To validate the results, a 4-fold approach was used, whereas the training set was randomly divided into 4 equal parts. Alternately, 3 parts were submitted to the training, and 1 was used for control.

When the training was complete, we calculated the F1-scores for 4 folds of this model and obtained the following values: 0.76, 0.82, 0.79, and 0.62, respectively. The mean F1-score for 4 folds of our model was 0.75.

### I. USE OF TRAINED ARTIFICIAL NEURAL NETWORK

The marking in Aperio is stored for each gigapixel image as a file in .xml format. A trained neural network allows to mark each patch on a gigapixel image of uveal melanoma or on a selected part of the image and present such machine-aided marking as an .xml file. In the .xml file, each marking color corresponding to a single class (predominant cell elements) is represented as a list of polygons described as an enumeration of its boundary points.

This marking method is very similar to the method used by pathologists to assess the cell population ratios judging by predominant cells in a number of fields of vision in the light microscope (usually approximately 20), but it ensures rough assessment of the ratio, taking into account the tumor node as a whole.

The data to which the neural network responds may be presented as mark-ups to patches and gigapixel images. Mark-ups may be intensity maps, cells with their boundaries and the probability of belonging to a certain class, deconvolution maps with features marked which contributed to the decision to include a cell into a certain class.

As seen from Figure 1, the areas of most probable nuclei location are marked with red mark-up and those of least probable location with blue mark-up. Figure 2 shows another variant of a visual mark-up

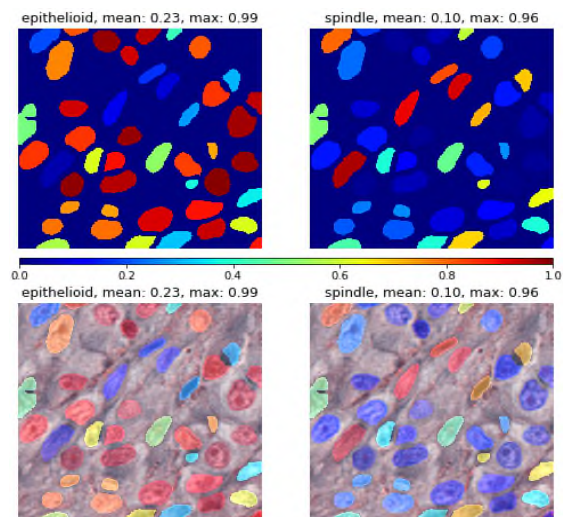


Figure 2. A color chart of the probability of cell belonging to a certain class

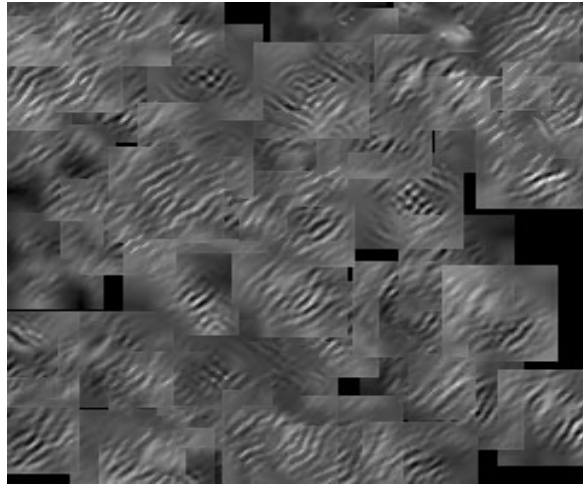


Figure 3. Deconvolution Map

presentation: a color chart of the probability of cell belonging to a certain class, where a bluish color represents the least probability and a reddish color corresponds to the highest probability. The last but the most diverse variant of data presentation is a map of contributions into the decision to include a cell into a certain class. Figure 3 shows an example of a deconvolution map for spindle-shaped and epithelioid cells. The patches show that spindle-shaped cells look like parallel folds rising above the plane of probability. Epithelioid cells are broken rounded folds. While comparing maps of contributions from parallel filters, it is obvious that higher probability folds for one class correlate with lower probability for the other. It can be assumed that this pair of filters mirrors inherent cell geometry, where epithelioid cells have a rounded nucleus and sphere-like shape and spindle-shaped cells have elongated nucleus and shape. A Web-based interface where anyone can upload a gigapixel image and see its machine-aided interpretation with a mentioned mark-up is being developed.

## II. CONCLUSION AND FUTURE WORK

Even small groups of patients may be used in digital pathology for training in convolution neural networks. This is possible due to the fact that each gigapixel image contains several thousand smaller images – patches, which in turn have two-three dozens of cells – training units. Our further work will be dedicated to training set extension and tests of images not included in the training sample.

The mean fold F1-score was 0.75. The result may seem unassertive if we do not take into consideration the fact that images in training sample very often had cells from another class. This aspect is very difficult to eliminate in pathology. The fact that machine-aided cell marking quite often contradicts the initial patches marking allows to assume that the classification accuracy is higher than this figure. Acquisition of more images with uniform cellular composition will allow us to assess more accurately the metrics of the classifier. In our opinion, the most appropriate mark-up to explain the differences between various types of

cells is color mark-up with cell boundaries and the probability of belonging to a certain class. Even an experienced pathologist sometimes finds it difficult to differentiate between spindle-shaped and epithelioid cells. Thus, it can be assumed that there are a number of cell subtypes which are similar to cell classes. The presentation of each cell as corresponding to a certain class (with the probability indicated) allows us to visualize this trend.

Mark-ups in the form of contribution maps are more appropriate for a research work and advanced pathologists training. Their non-obviousness makes their use in specialist training possible only with explanations.

We assume that the best solution for processed data demonstration is a Web-based interface in a browser with two synchronized windows, where one window shows raw data and the other window demonstrates the results of the functioning neural network (predicted classes, cells with their boundaries and the probability of belonging to a certain class, maps of features which contributed to the decision to include a cell into a certain class).

Although our work is devoted to the visualization of cellular signs of uveal melanoma, this approach can be used for automated pathomorphological diagnosis of uveal melanoma, which requires further study of the material base and methodology.

## REFERENCES

- [1] A. D. Singh, M. E. Turell, and A. K. Topham, "Uveal Melanoma: Trends in Incidence, Treatment, and Survival," *Ophthalmology*, Vol. 118(9), pp. 1881–1885, 2011, doi:10.1016/j.ophtha.2011.01.040
- [2] D. Lorenzo et al., "Prognostic Factors and Decision Tree for Long-Term Survival in Metastatic Uveal Melanoma," *Cancer Research and Treatment*, Vol. 50(4), pp. 1130–1139, 2018, doi:10.4143/crt.2017.171
- [3] I. W. McLean, W. D. Foster, L.E. Zimmerman, and J. W. Gamel, "Modifications of Callender's Classification of Uveal Melanoma at the Armed Forces Institute of Pathology," *American Journal of Ophthalmology*, Vol. 195, pp. lvi–lx, 2018, doi:10.1016/j.ajo.2018.08.025
- [4] S. Kaliki, C. Shields, and J. Shields, "Uveal melanoma: Estimating prognosis," *Indian Journal of Ophthalmology*, Vol. 63(2), p.93, 2015, doi:10.4103/0301-4738.154367
- [5] P. Khosravi, E. Kazemi, M. Imielinski, O. Elemento, and I. Hajirasouliha, "Deep Convolutional Neural Networks Enable Discrimination of Heterogeneous Digital Pathology Images," *EBioMedicine*, 2018, Vol. 27, pp. 317–328, doi:10.1016/j.ebiom.2017.12.02662.
- [6] J. T. Kwak, S. M. Hewitt, S. Sinha, and R. Bhargava, "Multimodal microscopy for automated histologic analysis of prostate cancer," *BMC Cancer*, 2011, Vol. 11(1), pp. 1-16, doi:10.1186/1471-2407-11-6263.
- [7] P. W. Hamilton et al., "Automated tumor analysis for molecular profiling in lung cancer," *Oncotarget*, 2015, Vol. 6(29), pp. 27938-27952, doi:10.18632/oncotarget.4391.
- [8] L. W. Wang et al., "Computer-Based Image Studies on Tumor Nests Mathematical Features of Breast Cancer and Their Clinical Prognostic Value," *PLoS ONE*, 2013, Vol. 8(12), p. e82314, doi:10.1371/journal.pone.0082314.
- [9] K. Bruno et al., "Deep learning for classification of colorectal polyps on whole-slide images," *PLoS One*, 2013, Vol. 8(12), p. e8231466, doi: 10.4103/jpi.jpi\_34\_17

- [10] A. Janowczyk et al., "High-Throughput Biomarker Segmentation on Ovarian Cancer Tissue Microarrays via Hierarchical Normalized Cuts," *IEEE Transactions on Biomedical Engineering*, 2012, Vol. 59(5), pp. 1240–1252, doi:10.1109/tbme.2011.2179546
- [11] C. Belmar-Lopez et al., "Uveal vs. cutaneous melanoma. Origins and causes of the differences," *Clinical and Translational Oncology*, 2008, Vol. 10(3), pp. 137–142, doi:10.1007/s12094-008-0170-4
- [12] A. Effland et al., "Joint reconstruction and classification of tumor cells and cell interactions in melanoma tissue sections with synthesized training data," *International Journal of Computer Assisted Radiology and Surgery*, 2019, Vol. 14(4), pp. 587-599, doi:10.1007/s11548-019-01919-z
- [13] E. Rexhepaj et al., "A Texture Based Pattern Recognition Approach to Distinguish Melanoma from Non-Melanoma Cells in Histopathological Tissue Microarray Sections," *PLoS ONE*, 2013, Vol. 8(5), pp. e62070, doi:10.1371/journal.pone.0062070
- [14] C. Liu et al., "SetSVM: An Approach to Set Classification in Nuclei-based Cancer Detection," *IEEE Journal of Biomedical and Health Informatics*, 2019, Vol. 23(1), pp. 351-361, doi:10.1109/jbhi.2018.2803793
- [15] L. Wang, W. Li, and Y. Kang, "Data Fusion Network for Instance Segmentation," *Lecture Notes in Computer Science*, 2018, pp. 175–182, doi:10.1007/978-3-030-01078-2